Non-LTE Radiation Transport in Moderate Density Plasmas

J.J. MacFarlane, P. Wang, and G.A. Moses

January 1990

UWFDM-821

Lasers & Part. Beams 8 (1990) 729.

FUSION TECHNOLOGY INSTITUTE

UNIVERSITY OF WISCONSIN

MADISON WISCONSIN

Non-LTE Radiation Transport in Moderate Density Plasmas

J.J. MacFarlane, P. Wang, and G.A. Moses

Fusion Technology Institute
University of Wisconsin
1500 Engineering Drive
Madison, WI 53706

http://fti.neep.wisc.edu

January 1990

UWFDM-821

Lasers & Part. Beams 8 (1990) 729.

ABSTRACT

We present results from non-LTE line radiation transport calculations for high-temperature, optically thick plasmas with densities ~ 10^{16} — 10^{20} ions/cm^3. The calculations are based on an escape probability radiative transport model in which the atomic rate equations are solved self-consistently with the radiation field. Steady-state ionization and excitation populations are determined by detailed balancing of atomic processes, with photoexcitation effects included. Atomic data are computed using a combination of Hartree-Fock, semiclassical impact parameter, and distorted wave calculations. Our results indicate that the reabsorption of line radiation significantly alters the level populations and reduces the radiation flux from several types of fusion-related plasmas. We also compare our results with those obtained from multigroup radiation diffusion calculations, and discuss the ramifications of our results for ICF target chamber plasmas.

1. INTRODUCTION

Radiative emission and transport play a crucial role in the dynamics and energetics of many high-energy density laboratory plasma experiments. Such experiments are often performed to develop a better understanding of physical processes that are key issues in inertial confinement fusion (ICF) research. Theoretical analysis, in conjunction with experiments, can significantly increase our knowledge base in areas such as equation of state physics, radiative transfer, ion and laser beam energy deposition, ablation physics, and atomic processes. These processes play a major role not only in the physics of ICF target implosions (Arnold and Meyer-ter-Vehn 1987; Tahir and Long 1986), but also in such areas as plasma channels used for transporting light ion beams to ICF targets (Moses et al. 1988), microfireball formation and expansion in target chamber background gases (Moses et al. 1985), and target chamber first wall response to target explosions (Badger et al. 1989).

In recent years, several studies (Duston & Davis 1980; 1981; Rogerson et al. 1985) have shown that high-temperature, moderate-to-high density (n ~ 10^{19} - 10^{22} ions/cm^3) laboratory plasmas are not in local thermodynamic equilibrium (LTE). For instance, Duston and Davis

(1981) have shown that the radiative properties of plasmas which are optically thick to line radiation are not well-described by either "coronal" or LTE plasmas. This results from the fact that line radiation (particularly that of line cores) is absorbed before it escapes the plasma. Reabsorption affects both the total intensity of line radiation escaping a plasma and the observed line shapes. Thus, it is crucial that non-LTE effects be considered when attempting to deduce plasma conditions from experimental radiation spectra.

The fact that the radiation field can significantly affect the properties of a plasma severely complicates the problem of modelling — and hence developing a better understanding of –– laboratory plasmas. This is because the opacities are altered by the photon-induced redistribution of the level populations, which in turn affects the radiation field. Because of this feedback mechanism, the atomic rate equations and radiation field must be evaluated self-consistently. The problem becomes particularly cumbersome when high-Z (Z = atomic number) materials are involved because of the large number of ionization and excitation levels that must be considered. For these reasons, theoretical calculations have often neglected the influence of the radiation field on the level populations.

In this paper, we describe a model for computing line radiative transfer in moderate density plasmas, and present results for plasmas that expand a range of temperatures and densities that typifies those expected in high-yield ICF target chambers. We use the term "moderate" to denote densities that are below those for which interparticle potentials become important ($n \lesssim 10^{22}$ cm^{-3}), but still high enough that collisional deexcitation and recombination effects cannot be neglected ($n \gtrsim 10^{15}$ cm^{-3}). The calculations are based on an escape probability radiation transport model in which the atomic rate equations are solved self-consistently with the radiation field (Apruzese et al., 1980). In this model, an angle- and frequency-averaging technique is used which allows the simultaneous, yet computationally efficient, solution of the radiation field and atomic rate equations. Steady-state ionization and excitation populations are determined by detailed balancing. A combination of Hartree-Fock, semiclassical impact parameter, and distorted wave models is used to compute atomics physics data. The atomic processes considered are: photoexcitation,

collisional excitation and deexcitation, spontaneous and stimulated emission, collisional ionization and recombination, and radiative and dielectronic recombination.

We shall also discuss the ramifications of our results to 2 areas of importance to ion-driven fusion: (1) Z-pinch plasma channels, which are used for transporting light-ion beams from diodes to ICF targets; and (2) radiation emission from high-temperature plasmas ("microfireballs") which are created as high-yield target explosions deposit energy within target chamber background gases. We will show that "line trapping" — i.e., the reabsorption of line radiation in optically thick line cores — can significantly affect the level populations and plasma emission rates. We also present comparisons of our results with those from multigroup radiation diffusion calculations. The comparisons suggest that by not accounting for the reabsorption of line radiation and influence of the radiation field on the level population, diffusion models can significantly overestimate emission rates from non-LTE plasmas.

2. NON-LTE RADIATIVE TRANSFER MODEL

When a plasma is in LTE, its properties (e.g., internal energy, opacity) depend only on the local temperature and density, and are independent of the radiation field. However, it has been shown that quite often the plasmas created in laboratory experiments are far from LTE (Duston & Davis 1981). The same has recently been shown to be true for plasmas created in high-gain ICF target chambers (MacFarlane et al. 1989a; 1989b). A major reason for the departure from LTE is that as plasmas become optically thick to line radiation, the radiation field can significantly alter the atomic level populations. When this occurs, reliable predictions for the plasma radiative properties can only be obtained by solving the atomic rate equations self-consistently with the radiation field. Any model that does not account for this coupling can lead to inaccurate results for both plasma energetics and the diagnoses of plasma conditions from experimental spectra.

To simulate radiation transport in non-LTE plasmas, we use a model similar to that developed by Apruzese et al. (1980). This model is based on escape probability methods which allow the multilevel atomic rate equations and radiative transfer equation to be solved self-consistently.

Frequency-averaged escape probabilities for line photons (with Doppler, Lorentz, or Voigt profiles) are calculated using empirical fits to exact numerical results. Angle-averaged zone-to-zone coupling coefficients are calculated to determine the photoexcitation and spontaneous emission rate coefficients. The techniques employed have been shown to lead to reliable results for a variety of line profiles, geometries, and optical depths (Apruzese et al. 1980; Apruzese 1981; 1985). Because this model requires relatively little computer time, it can be coupled with hydrodynamics codes to provide a powerful computational tool for simulating rapidly changing, non-LTE plasmas.

We shall briefly summarize the major features of the radiative transfer model here. More detailed descriptions are provided elsewhere (Apruzese et al. 1980; Apruzese 1981; 1985; MacFarlane et al. 1990). The essence of the model can best be explained by examining the case of a 2-level atom. Let N_u^i and N_l^i denote the upper and lower level populations of zone i, respectively. The steady-state populations are determined by solving the atomic rate and mass conservation equations (see, e.g., Mihalas 1978):

$$\frac{dN_u^i}{dt} = 0 \; = N_l^i \; (C_{lu}^i + B_{lu} \, \bar{J}^i) - N_l^i \; (A_{ul} + C_{ul}^i + B_{ul} \, \bar{J}^i) \qquad (1)$$

and

$$N_l + N_u = N_{tot} \, , \qquad (2)$$

where C_{lu} and C_{ul} are the collisional populating and depopulating rate coefficients, respectively, A_{ul} is the spontaneous decay rate, B_{lu} and B_{ul} are the Einstein stimulated absorption and emission coefficients, and $\bar{J}$ is the mean intensity averaged over the line profile. In the escape probability model, the sum of the stimulated absorption (photoexcitation) and stimulated emission rates can be expressed in terms of zone-to-zone "coupling coefficients," Q, such that:

$$N_l^i \; B_{lu}^i \; \bar{J}^i - N_u^i \, B_{ul} \; \bar{J}^i = \sum_{j=1}^{N_D} N_u^j \, A_{ul} \; Q^{ji} \, . \qquad (3)$$

The quantity Q^{ji} represents the probability a photon emitted in zone j is absorbed in zone i. The product $N_u^j A_{ul}$ simply represents the number of spontaneous decays in zone j per unit time.

The coupling coefficients are evaluated using the following frequency and angle-averaging techniques. Let $P_e(\tau_o)$ represent the mean probability — averaged over the line profile — that a photon emitted at some point will traverse a line center optical depth τ_o before being reabsorbed. Then,

$$P_e(\tau_o) = \int_0^\infty \phi(\nu)\, exp(-\tau_o\, \phi(\nu)/\phi(\nu_o))\, d\nu\,, \tag{4}$$

where ϕ_ν is the line profile and ν_o is the line center frequency. For bound-bound transitions we assume "complete redistribution." Therefore, the absorption and emission profiles are identical.

The coupling coefficient for photons emitted in zone i and absorbed in zone j can be written as:

$$Q^{ij} = \frac{1}{\tau_i} \int_0^{\tau_i} [P_e\,(\tau_B + \tau) - P_e\,(\tau_B + \tau_j + \tau)]\, d\tau\,, \tag{5}$$

where τ_i, τ_j, and τ_B represent the line center optical depths of the emitting zone i, the absorbing zone j, and the region between zones i and j, respectively. These optical depths are computed along a "mean diffusivity angle," $\bar{\theta}$, with respect to the radial direction. Apruzese (1981) showed that using a value of $\cos\bar{\theta} \approx 0.51$, the escape probability model reproduces exact 2-level atom solutions quite well for a variety of geometries and optical depths. Thus, a high degree of computational efficiency is achieved for only a modest sacrifice in accuracy. For multilevel atomic systems, $N_D \times N_L$ atomic rate equations must be solved simultaneously. In addition, since the optical depths in Eq. (5) depend nonlinearly on the level populations, an iterative technique is used to determine the populations.

3. ATOMIC PHYSICS CALCULATIONS

In our radiative transport model, every state is coupled to the ground state of the next higher ionization stage by collisional ionization, collisional recombination and radiative recombination. The adjacent ground states are also coupled by dielectronic recombination. The excited levels of a given ion are coupled to other excited levels and the ground state by electron collisional excitation and deexcitation, stimulated absorption and emission, and spontaneous radiative decay. Collisional coupling is complete in our calculations; thus we consider forbidden and spin-flip transitions as well as those which are electric dipole allowed.

In the calculations of atomic energy levels, the interaction between the atomic electrons is approximated by an LS-coupling scheme. The energy level and oscillator strength data is generated from Hartree-Fock calculations. We now describe the models by which the atomic rate coefficients are computed.

A. Excitation and Deexcitation

Three methods are employed for the calculation of excitation cross sections and rate coefficients. For all electric dipole allowed transitions, the excitation cross sections are calculated by using the semiclassical impact-parameter method (SCI) (Burgess and Summer 1976). A distorted wave model (DW) (Sobelman et al., 1981) is used to calculate the excitation cross sections of forbidden and spin-flip transitions for helium-like and lithium-like ions, while the orthogonalized function method (Beigman and Vainshtein, 1967) in the Born-Oppenheimer approximation (BOA) is used for other ions. The rate coefficients are obtained by averaging the cross-sections over a Maxwellian electron velocity distribution. The principle of detailed balance is applied to obtain the deexcitation rate coefficients from the excitation rate coefficients.

The reliability of stimulated and spontaneous emission rates depends directly on the accuracy of the oscillator strengths. In this study, only the electric dipole radiative transitions are considered. All oscillator strengths are generated by using Hartree-Fock methods. Table 1 lists a few selected oscillator strengths and compares them with the tables of Smith and Wiese (1971),

which is based on a combination of experimental data and calculations. Agreement is seen to be quite good.

Table 1. Oscillator Strengths for NeV

Transition	f^{HF}	f^{sw}
$2s^2 2p^2\ (^3P)$ - $2s^1 2p^3\ (^3P)$	0.108	0.13
(^1D)- (^1P)	0.150	0.17
$2s^2 2p^1 3s^1\ (^3P)$ - $2s^2 2p^1 3p^1\ (^3D)$	0.298	0.30
(^3P)- (^3P)	0.180	0.23
(^3P)- (^3S)	0.068	0.065
$2s^2 2p^1 3p^1\ (^3S)$ - $2s^2 2p^1 3d\ (^3P)$	0.416	0.42
(^3P)- (^3P)	0.125	0.10
(^3P)- (^3D)	0.350	0.32
(^1P)- (^1P)	0.147	0.15
(^1P)- (^1D)	0.283	0.29

B. Ionization and Recombination

The electron collisional ionization rate coefficients used in this study are calculated using the semi-empirical formula proposed by Burgess et al. (1983):

$$q = (2.17 \times 10^{-8}\ cm^3\ s^{-1})\ C \sum_j \zeta_j\ (I_H/I_j)^{3/2}\ (I_j/kT)^{1/2}\ E_1\ (I_j/kT)\ w_j\ , \qquad (6)$$

where the summation is over shells j of the initial ion, ζ_j is the effective number of electrons in j, l_j is the effective ionization energy of j, and $I_H = 13.6\ eV$. The parameter C is determined from

experimental data. For the cases in which experimental data are not available, the value of C is taken to be 2.3. The quantity $E_1(x)$ is the first exponential integral,

$$w_j = [\ln (1 + kT/I_j)]^{\beta/(1+kT/Ij)}$$

and

$$\beta = \frac{1}{4}\{[(100z + 91)/(4z + 3)]^{1/2} - 5\} .$$

Here z is the charge of the initial ion. This empirical formula has been shown to produce good agreement with crossed-beam experimental data over a wide range of conditions. The electron collisional recombination rate coefficient is obtained by using the principle of detailed balance.

The cross section for radiative recombination to the ith atomic level can be obtained from Milne's relation (Sobelman et al., 1981):

$$\sigma^r(\varepsilon) = \frac{g_i\,(I_i + \varepsilon)^2}{g_e g_+\,\varepsilon m_e c^2}\,\sigma^i(\varepsilon) \qquad (7)$$

where σ^i is the photoionization cross section, I_i is the ionization potential of the atom at ith state, ε is the kinetic energy of the incident electron, and g_e, g_i, and g_+ are the statistical weights of electron, combined ion, and uncombined ion, respectively. It is well known that direct application of the photoionization cross sections for hydrogenlike species to the low-lying states of multielectron atomic systems is unreliable. In our calculations, the photoionization cross sections are generated using the Hartree-Fock calculations. This is illustrated in Fig. 1, where the photoionization cross section of neutral Ne is shown as a function of wavelength. Shown with the Hartree-Fock (HF) results are curves representing experimental data (Marr and West, 1976) and hydrogenic ion cross sections. Note that the HF results are in much better agreement with the

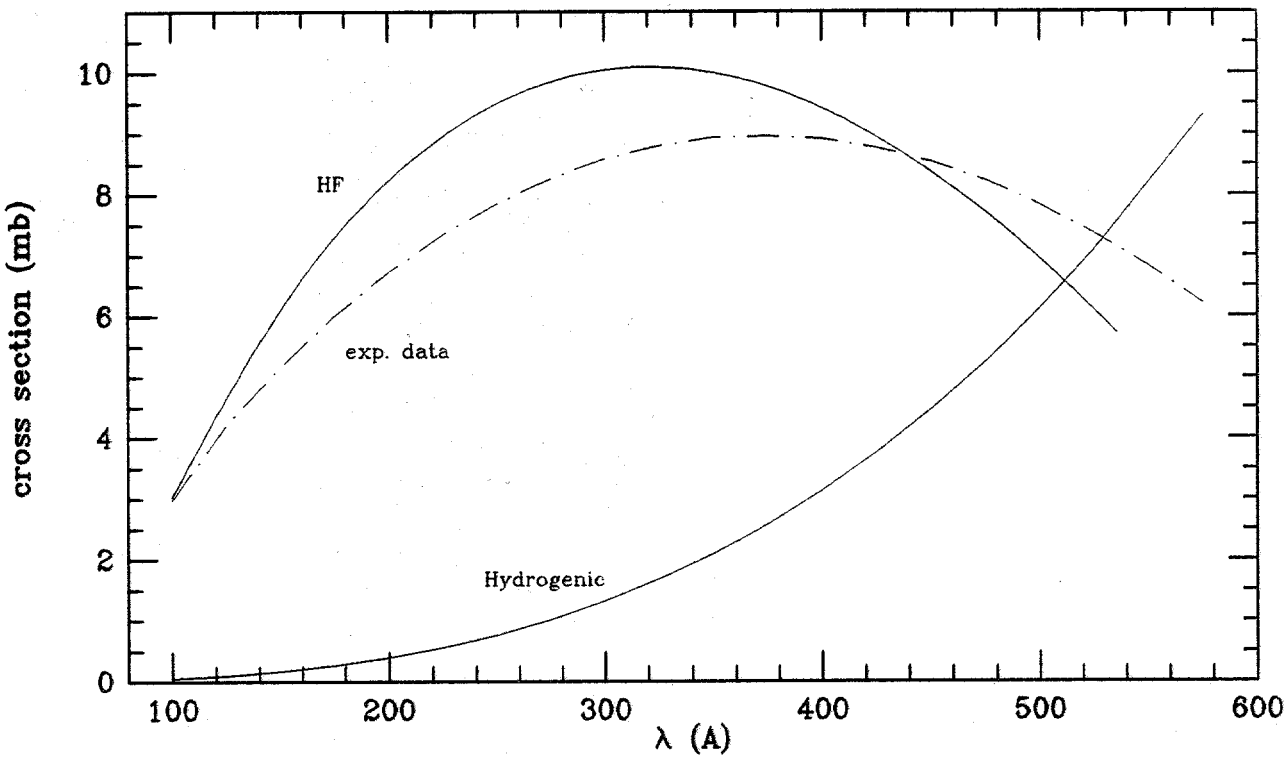

Fig. 1. Photoionization cross section for neutral Ne vs. wavelength. Hartree-Fock (HF) calculations are compared with experimental data (Marr and West, 1976) and hydrogenic ion approximation results. The photoionization cutoff wavelength is 575 Å (= 21.6 eV).

experimental data than the hydrogenic cross sections. The radiative recombination cross sections are used with the Maxwellian electron distribution to obtain the rate coefficient for radiative recombination to each atomic level.

As shown by Burgess and Seaton (1964), the dielectronic recombination rate in many cases can considerably exceed the radiative recombination rate. Therefore, in low density and high temperature plasmas, dielectronic recombination must be considered. We have calculated the dielectronic recombination rate coefficient using the Burgess-Merts model (Post et al., 1977). Figure 2 shows the dielectronic, radiative, and collisional recombination rates from NeIX to NeVIII as a function of electron temperature. It is clear from these results that dielectronic recombination becomes the dominate recombination process for this ion at temperatures $\gtrsim$ 200 eV.

4. RESULTS

We next present results from non-LTE radiative transfer calculations for plasmas with temperatures ~ 10^1 - 10^4 eV and densities ~ 10^{16} - 10^{20} ions/cm^3. These conditions are typical of those expected to occur within Z-pinch plasma channels and high-temperature microfireballs inside light ion-driven ICF target chambers (Moses et al. 1988). We have selected neon plasmas because inert gases have often been proposed for target chamber background gases. Calculations have been performed for plasmas with uniform densities and temperatures. The primary objectives of this study were to determine the influence of the radiation field on the atomic populations, and to get a preliminary assessment of the importance of line trapping in ICF target chamber plasmas.

We first consider the case of an optically thick, spherical Ne plasma with a uniform temperature of 250 eV, a uniform density of 3×10^{16} ions/cm^3, and a radius of 100 cm. (This density corresponds to a pressure of about 1 torr at room temperature, while the size is typical of a microfireball created by a high-yield target explosion.) At this density and temperature the Ne is predominantly in the H-like (NeX) and He-like (NeIX) ionization stages. The level structure considered for this calculation, which consists of 14 levels and 3 ionization stages, is shown in Fig. 3 (NeXI not shown). The number of spatial zones was 10.

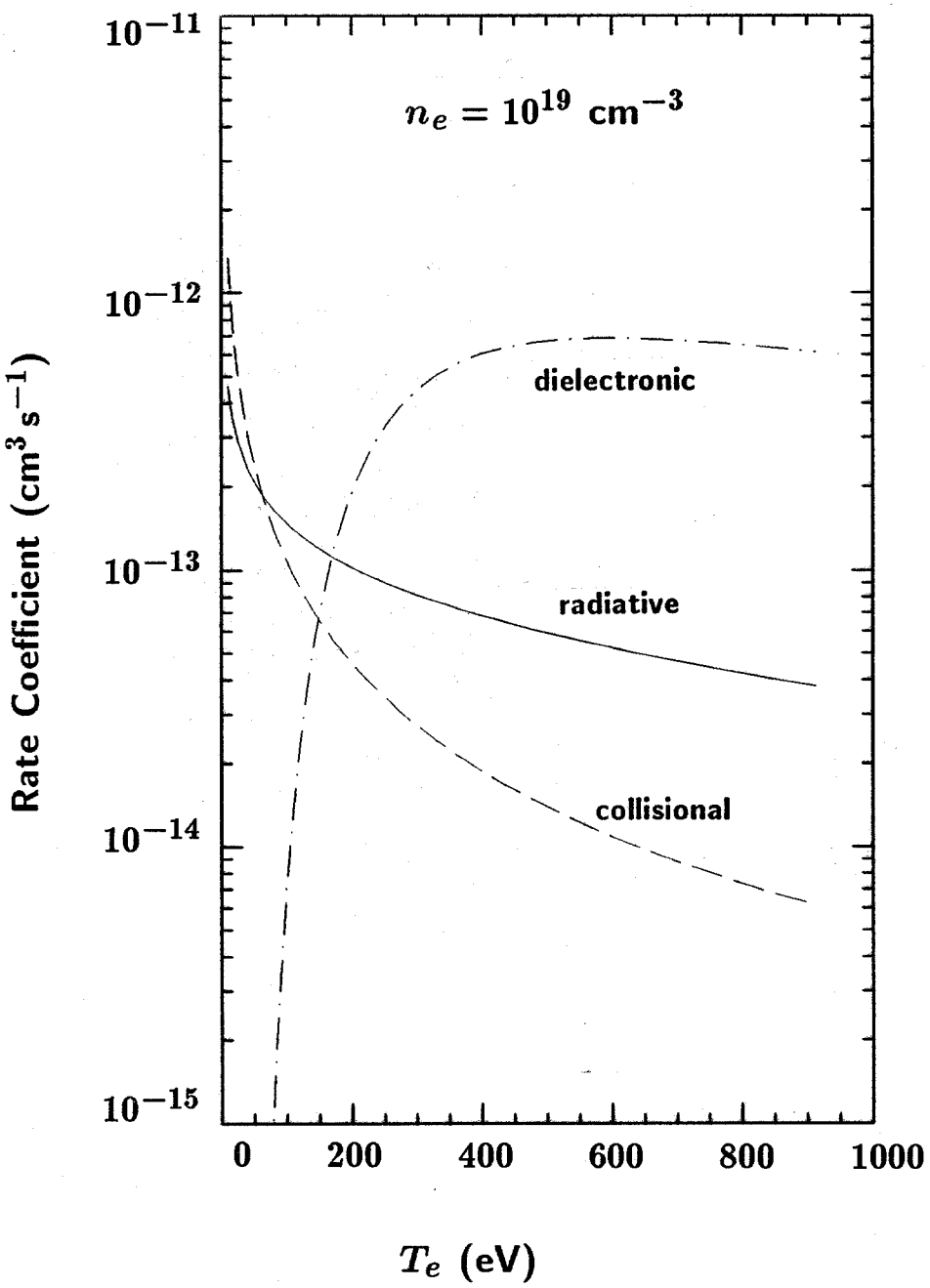

Fig. 2. Dielectronic, radiative, and collisional recombination rate coefficients for NeIX to NeVIII as a function of electron temperature. The electron density is 1 x 10^{19} cm^{-3}.

Figure 4 shows the populations for the NeIX and NeX as a function of radius in the plasma sphere. Note that even though the temperature and density are uniform throughout the plasma, the level populations can vary substantially because the radiation field is nonuniform. For some levels (e.g., $1s2p\,^1p$ (NeIX) and $n=2$ (NeX)) the excited state populations decrease by up to a factor of 10 near the plasma boundary. This occurs because of the lack of radiation incident on the outer boundary of the plasma. There is a relatively small gradient in the population of the $1s2p\,^1p$ level for NeIX because the transition with the ground state involves a change in the electron spin state.

Also shown in Fig. 4 are the populations for an optically thin Ne plasma at the same density and temperature (dashed curves). In this case, the photoexcitation rates are assumed to be zero and the populations are independent of the radiation field. Comparison of the optically thick and optically thin results shows that the radiation field can significantly alter the populations of the excited states. For instance, the $1s2p\,^1P$ (Ne IX) and $n=2$ (Ne X) populations are 2 to 3 orders of magnitude higher near the slab center for the optically thick case.

Figure 5 shows the total line power coefficients (≡ power density / $n_e\, n_{tot}$) for optically thin Ne plasmas as a function of the electron temperature for densities ranging from 3×10^{16} to 3×10^{20} ions/cm^3. At low densities ($<< 10^{16}$ ions/cm^3), the power coefficient becomes independent of the density because the collisional deexcitation and recombination rates become much smaller than their radiative counterparts. This is often referred to as the "coronal" regime. As the density increases, the excited state populations decrease due to the increased importance of collisionally-induced downward transitions.

Reabsorption effects in optically thick plasmas can be seen in Fig. 6. Here, the total line power for a Ne plasma sphere with $n = 3 \times 10^{16}$ ions/cm^3 is plotted as a function of the electron temperature. As the radius of the sphere increases from zero (optically thin case) to 100 cm, the total line power decreases by as much as an order of magnitude. This is because the line center optical depths become large (up to ~ 10^3 for R = 100 cm) and photons emitted from within the plasma interior are "destroyed" before they can escape.

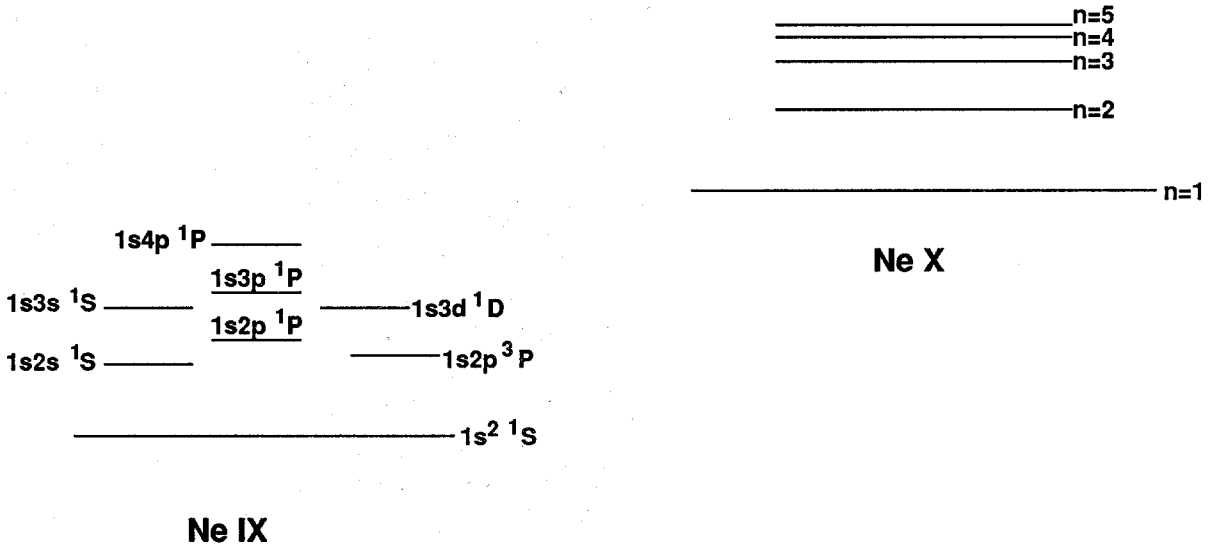

Fig. 3. Level structure considered for the NeIX and NeX ionization stages.

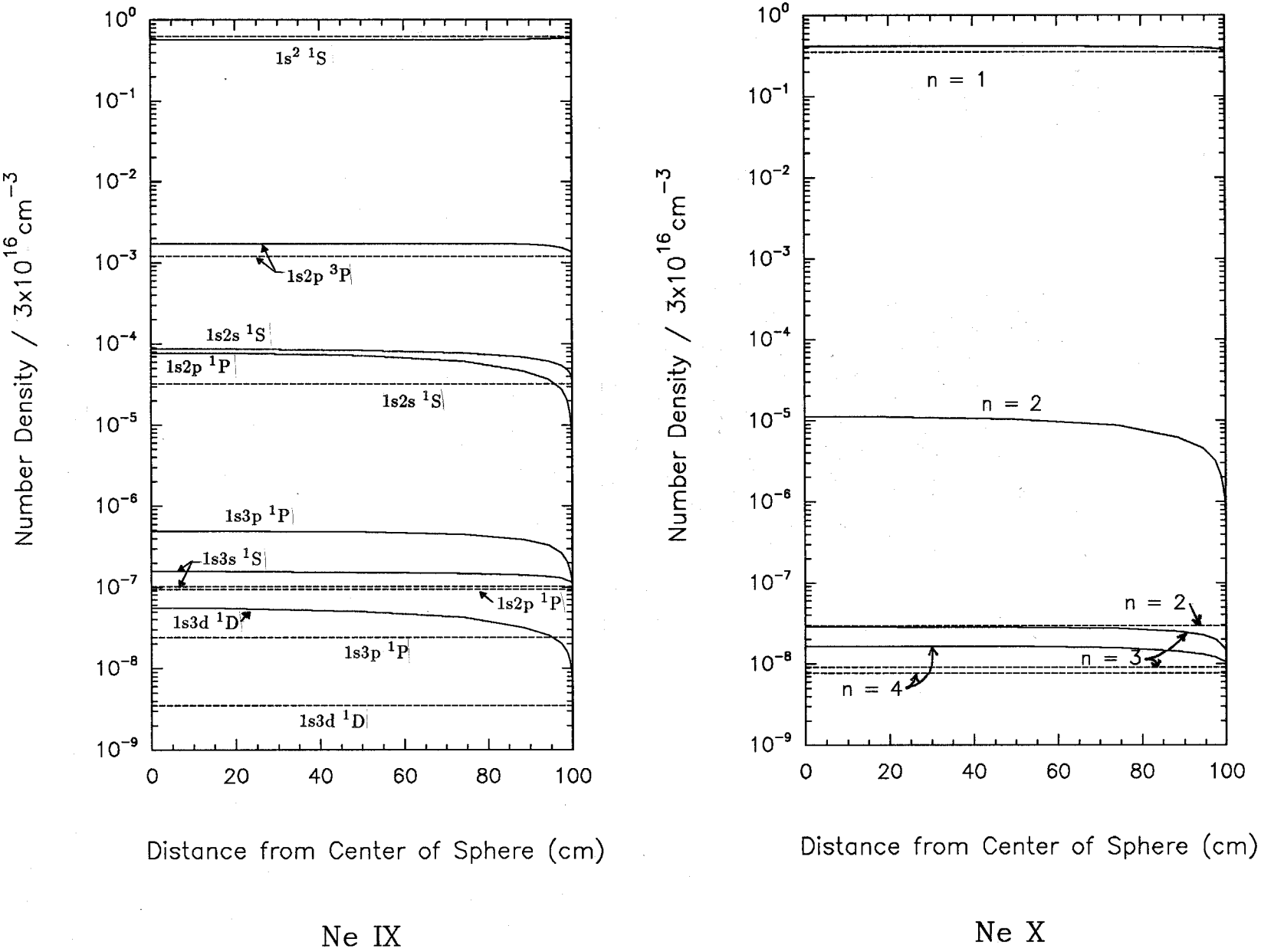

Fig. 4. Level population distributions in a 100 cm radius Ne plasma sphere with $T_e = 250$ eV and $n = 3 \times 10^{16}$ ions/cm^3. Dashed lines indicate optically thin populations.

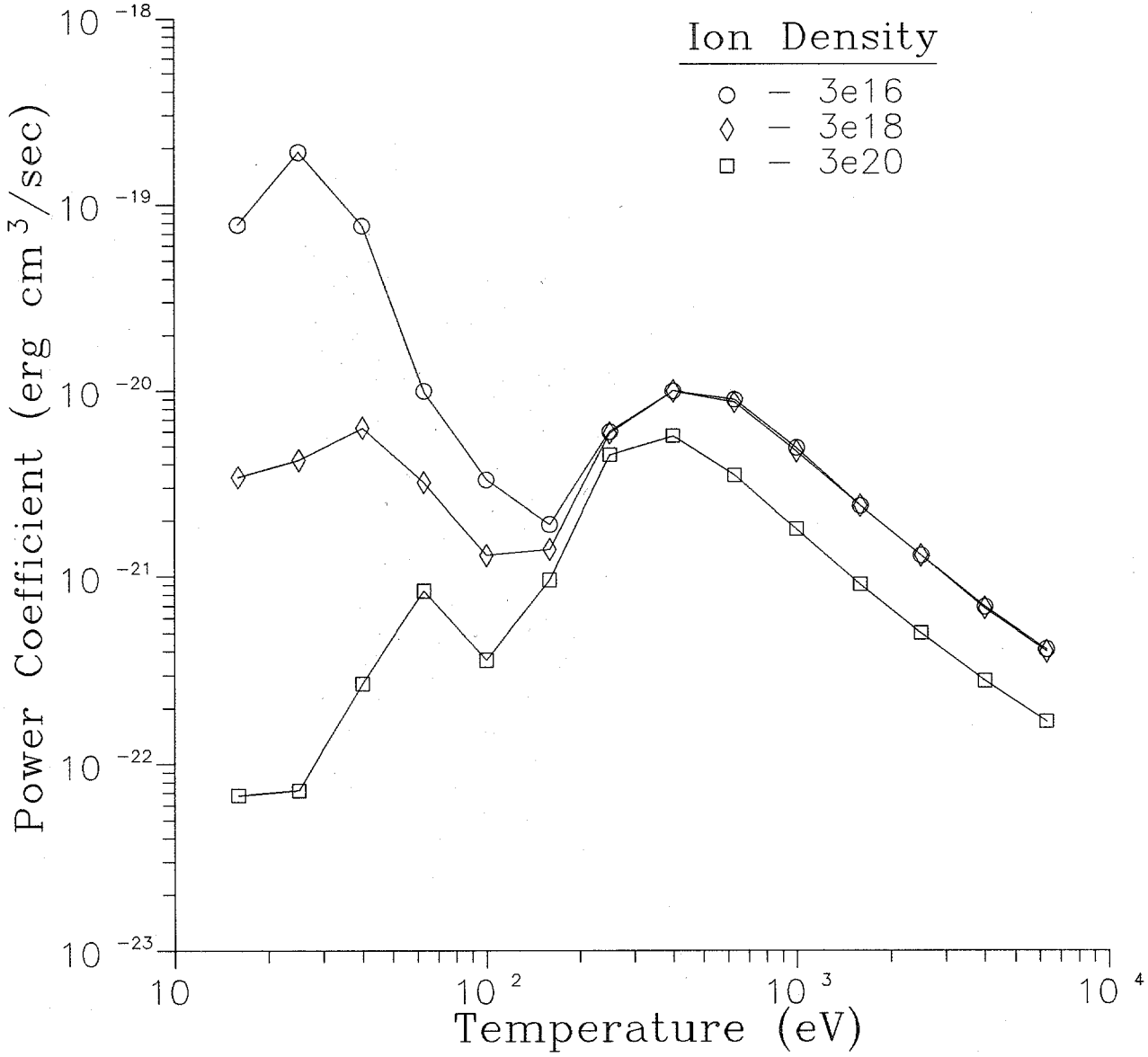

Fig. 5. Total line power coefficients of optically thin Ne plasmas at ion densities of 3 x 10^{16} cm^{-3} (top), 3 x 10^{18} cm^{-3}, and 3 x 10^{20} cm^{-3} (bottom).

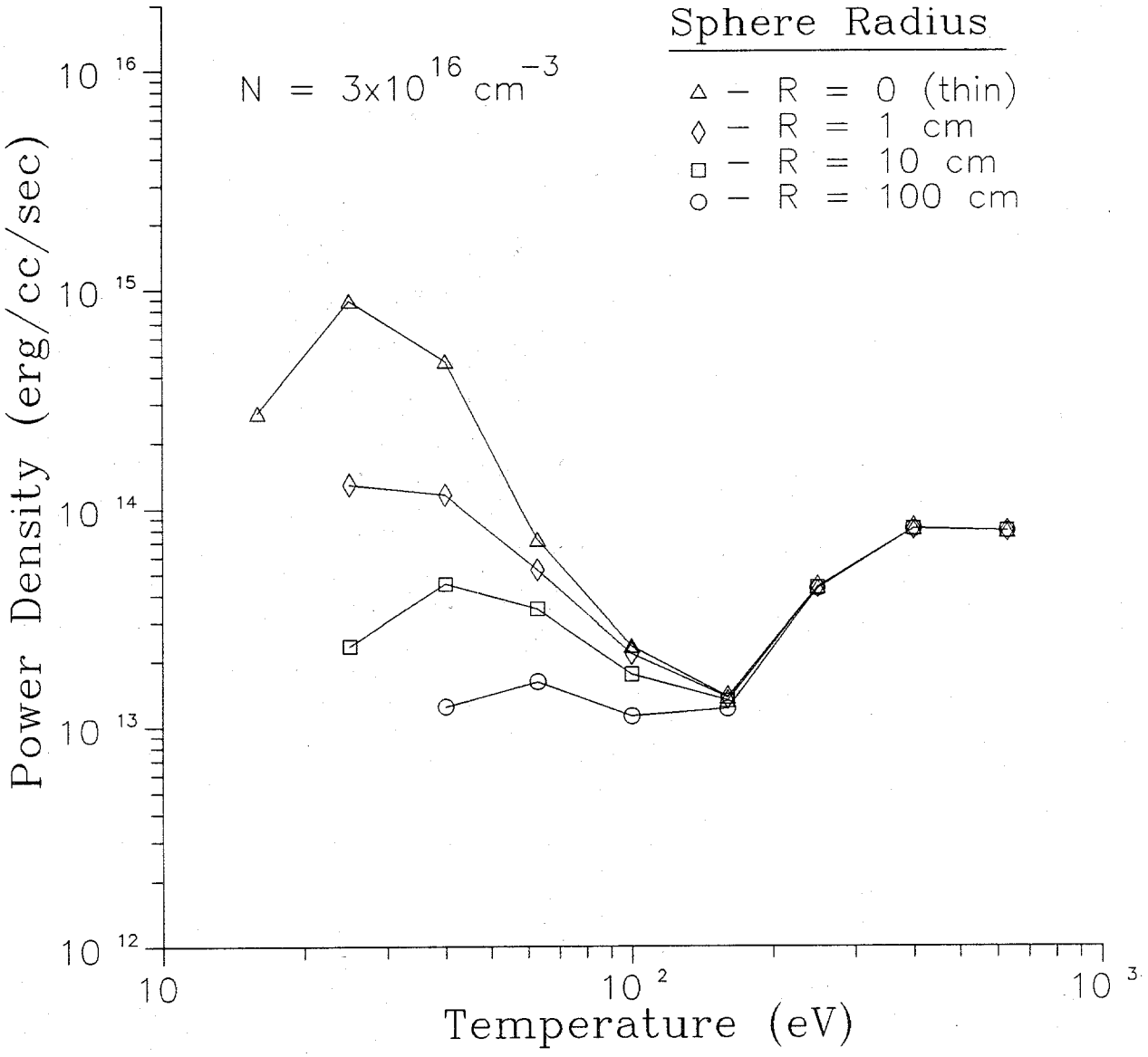

Fig. 6. Total line emission power densities for optically thick Ne plasma spheres. The ion density in each case was 3 x 10^{16} cm^{-3}. The radius of the plasma sphere ranged from zero ("thin" case, top curve) to 100 cm (bottom curve).

We have also compared our results with multigroup radiation diffusion calculations (Peterson et al., 1988). Fig. 7 shows the power densities — scaled to the thin power densities to mitigate differences that arise due to atomic physics data — for spherical Ne plasmas with radii ranging from 1 to 100 cm. In each case the plasma has a uniform density of 3×10^{16} ions/cm^3. The plasma temperatures are 40 eV and 100 eV in the top and bottom figures, respectively. At 40 eV, the multigroup diffusion power densities are about a factor of 4 higher than the non-LTE escape probability results for the 1 cm case, and more than an order of magnitude higher for the 100 cm case. At 100 eV, the discrepancies are somewhat smaller, with the diffusion results ranging up to about a factor of 2 higher for the 100 cm case. Note that as the plasma radii — and therefore the total line optical depths — increase, the discrepancies between the two models increase. These results suggest that the radiation diffusion calculations, which do not consider either the influence of the radiation field on the atomic populations or the reabsorption of line radiation properly, can significantly overestimate the radiation flux escaping optically thick, moderate density plasmas.

These conclusions may have important implications for ICF target chamber plasmas. For example, in the LIBRA light ion beam reactor design study (Moses et al., 1988), a low-Z background gas (He) was used because it was predicted that higher-Z gases would not produce magnetic fields of sufficient strength to confine the ion beam as it propagates from the diode to the target. This conclusion was based on radiation-magnetohydrodynamics calculations which predicted that radiatively-driven expansion (RDE) in higher-Z plasma channels leads to larger channels and weaker magnetic fields. In these calculations, radiation was transported using multigroup radiation diffusion models. Our present non-LTE radiative transfer calculations now suggest, however, that reabsorption of line radiation may significantly reduce RDE effects and result in stronger magnetic fields for higher-Z gases. It would be advantageous to use higher-Z gases to transport light ion beams to the target because the gas would provide significantly greater protection for the chamber walls from the target X-rays.

Our non-LTE results also suggest that the radiative flux from microfireballs will be lower than predicted from radiation diffusion models. This is important because the radiative heat flux on

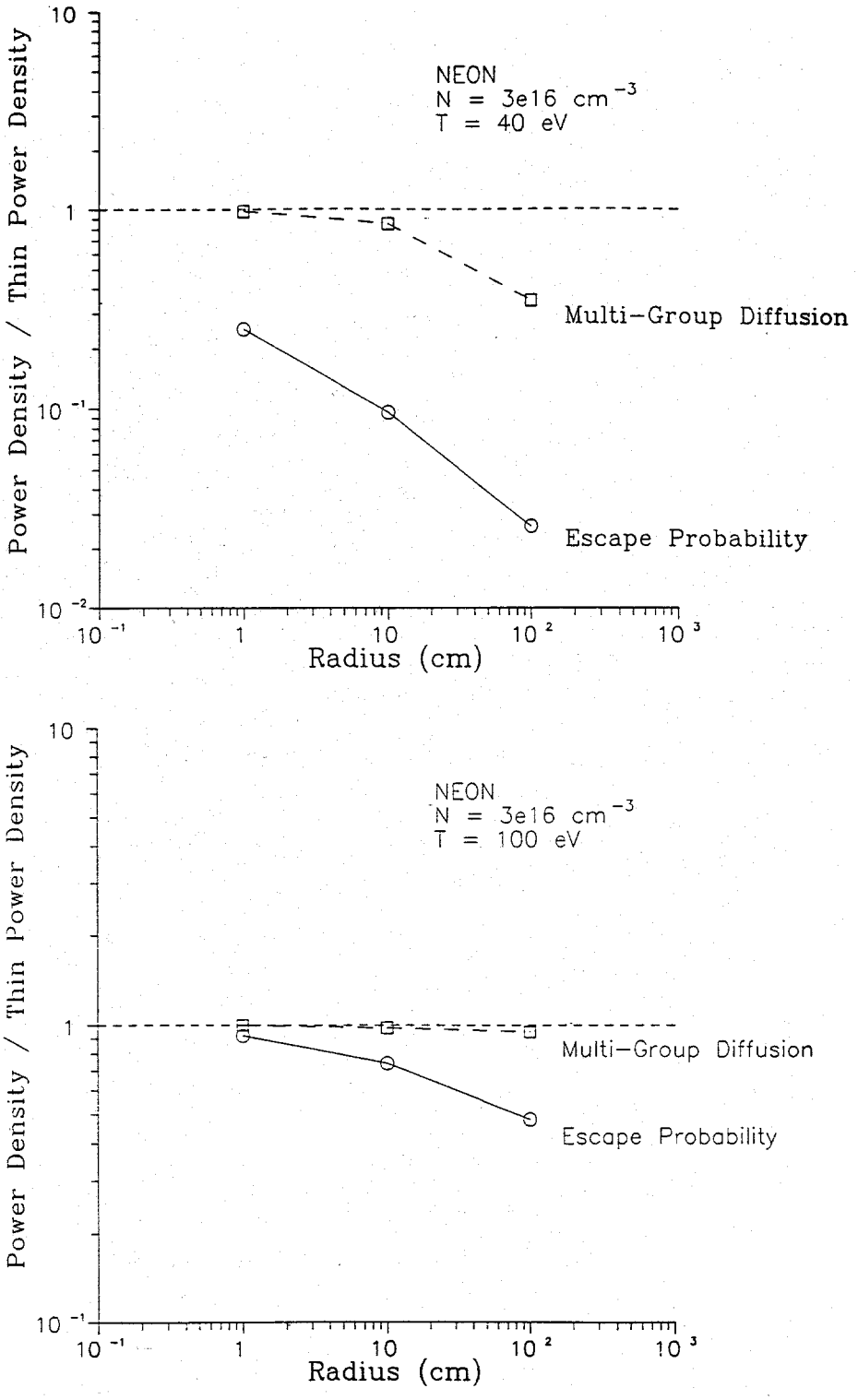

Fig. 7. Comparison of scaled power densities computed using non-LTE escape probability model and multigroup radiation diffusion model. Calculations are for spherical Ne plasmas with n = 3 x 10^{16} ions/cm^3 at T = 40 eV (top) and T = 100 eV (bottom).

the first wall is sometimes sufficiently high to produce potentially damaging thermal stresses in the wall and excessive erosion rates. To counteract this, some target chamber designs have been proposed in which massive "debris shields," such as a 1 kg shell of frozen nitrogen (Tabak 1989), are used to reduce the high heat fluxes. It seems possible, however, that line trapping alone will cause fluxes to be low enough that such elaborate protection measures are not necessary. Thus, line reabsorption effects may prove to be very beneficial in reducing the radiative heat flux on the target chamber first wall.

5. SUMMARY

We have presented results from non-LTE line radiative transfer calculations for high-temperature, moderate-density plasmas. We find that for conditions expected for high-yield ICF target chamber plasmas — specifically those within Z-pinch plasma channels and high-temperature microfireballs — the radiation field can dramatically alter the atomic level populations. In addition, we find that the reabsorption of radiation by the line cores results in a significant reduction in the radiation flux escaping these plasmas. Comparisons with multigroup radiation diffusion calculations suggest the diffusion models can grossly overestimate the radiative power emitted by optically thick plasmas.

ACKNOWLEDGEMENTS

The authors gratefully acknowledge support from Kernforschungszentrum Karlsruhe (KfK) through Fusion Power Associates. Computing support has been provided in part by the U.S. National Science Foundation through the San Diego Supercomputer Center.

REFERENCES

APRUZESE, J. P., DAVIS, J., DUSTON, D., & WHITNEY, K. G. 1980 *J. Quant. Spectrosc. Radiat. Transfer* **23**, 479.

APRUZESE, J. P. 1981 *J. Quant. Spectrosc. Radiat. Transfer* **25**, 419.

APRUZESE, J. P. 1985 *J. Quant. Spectrosc. Radiat. Transfer* **34**, 447.

ARNOLD, R. & MEYER-TER-VEHN, J. 1987 *Rep. Prog. Phys.* **50**, 559.

BADGER, B., PETERSON, R. R., ENGELSTAD, R. L., SAWAN, M. E., KHATER, H., MacFARLANE, J. J., MOSES, G. A., & LOVELL, E. G. 1989 University of Wisconsin Fusion Technology Institute Report UWFDM-768, Madison, WI.

BEIGMAN, I.L. & VAINSHTEIN, L.A. 1967 *Sov. Phys. JETP* **25**, 119

BURGESS, A. & CHIDICHCHIMO, M.C. 1983 *Mon. Not. R. Astr. Soc*. **203**, 1269.

BURGESS, A. & SEATON, M.J. 1964 *Mon. Not. R. Astr. Soc*. **125**, 355.

BURGESS, A. & SUMMER, H.P.1976 *Mon. Not. R. Astr. Soc*. **174**, 345.

DUSTON, D. & DAVIS, J. 1980 *Phys. Rev. A* **21**, 1664.

DUSTON, D. & DAVIS, J. 1981 *Phys. Rev. A* **23**, 2602.

MacFARLANE, J. J., MOSES, G. A., & PETERSON, R. R. 1989a *Nucl. Fusion* **29**, 27.

MacFARLANE, J. J., WANG, P., YASAR, O., & MOSES, G. A. 1989b *Bull. Amer. Phys. Soc*. **34**, 2151.

MacFARLANE, J. J., WANG, P., & MOSES, G. A. 1990 University of Wisconsin Fusion Technology Institute Report UWFDM-821, Madison, WI.

MARR, G.V. & WEST, J.B. 1976 *At. Data Nucl. Data Tables* **18**, 497.

MIHALAS, D. 1978 Stellar Atmospheres, Second Edition (Freeman, New York).

MOSES, G. A., PETERSON, R. R., & McCARVILLE, T. J. 1985 *Comput. Phys. Commun*. **36**, 249.

MOSES, G. A., et al. 1988 Proceedings of the Beams '88 Conference, Karlsruhe, FRG.

PETERSON, R.R., MacFARLANE, J.J., & MOSES, G.A. 1988 University of Wisconsin Fusion Technology Institute Report UWFDM-670, Madison, WI.

POST, D.E., JENSEN, R.V., TARTER, C.B., GRASBERGER, W.H., & LOKKE, W.A. 1977 *At. Data Nucl. Data Tables* **20**, 397.

ROGERSON, J. E., CLARK, R. W., & DAVIS, J. 1985 *Phys. Rev. A* **31**, 3323.

SMITH, M.W. & WIESE, W.L. 1971 *Ap. J.* **23**, 103.

SOBELMAN, I.I., VAINSHTEIN, L.A., & YUKOV, E.A. 1981 Excitation of Atoms and Broadening of Spectral Lines (Springer-Verlag, New York).

TABAK, M. 1989 *Bull. Amer. Phys. Soc*. **34**, 2144.

TAHIR, N. A. & LONG, K. A. 1986 *Phys. Fluids* **29**, 1282.

FIGURE CAPTIONS

Fig. 1. Photoionization cross section for neutral Ne vs. wavelength. Hartree-Fock (HF) calculations are compared with experimental data (Marr and West, 1976) and hydrogenic ion approximation results. The photoionization cutoff wavelength is 575 Å (= 21.6 eV).

Fig. 2. Dielectronic, radiative, and collisional recombination rate coefficients for NeIX $\rightarrow$ NeVIII as a function of electron temperature. The electron density is 1×10^{19} cm^{-3}.

Fig. 3. Level structure considered for the NeIX and NeX ionization stages.

Fig. 4. Level population distributions in a 100 cm radius Ne plasma sphere with T_e = 250 eV and $n = 3 \times 10^{16}$ ions/cm^3. Dashed lines indicate optically thin populations.

Fig. 5. Total line power coefficients of optically thin Ne plasmas at ion densities of 3×10^{16} cm^{-3} (top), 3×10^{18} cm^{-3}, and 3×10^{20} cm^{-3} (bottom).

Fig. 6. Total line emission power densities for optically thick Ne plasma spheres. The ion density in each case was 3×10^{16} cm^{-3}. The radius of the plasma sphere ranged from zero ("thin" case, top curve) to 100 cm (bottom curve).

Fig. 7. Comparison of scaled power densities computed using non-LTE escape probability model and multigroup radiation diffusion model. Calculations are for spherical Ne plasmas with $n = 3 \times 10^{16}$ ions/cm^3 at T = 40 eV (top) and T = 100 eV (bottom).